# Supplementary Information

## Carbon Quantum Dot-Mediated Binary Metal-Organic Framework Nanosheets for efficient Oxygen Evolution at ampere-level current density in proton exchange membrane electrolyzers

Qianjia Ni,[a#] Shiyuan Zhang,[b#] Kang Wang,[a] Huazhang Guo,[a] Jiye Zhang,[c] Minghong Wu,[b,d] Liang Wang*[a,e]

[a]Institute of Nanochemistry and Nanobiology, School of Environmental and Chemical Engineering, Shanghai University, Shanghai 200444, P. R. China

[b]Shanghai Institute of Applied Radiation, Key Laboratory of Organic Compound Pollution Control Engineering (MOE), School of Environmental and Chemical Engineering, Shanghai University, Shanghai, 200444 P. R. China

[c]School of Materials Science and Engineering, Shanghai University, Shanghai, 200444 P. R. China

[d]College of Environment & Safety Engineering, Fuzhou University, Fuzhou 350108, P. R. China

[e]Shanghai Engineering Research Center of Organ Repair, Joint International Research Laboratory of Biomaterials and Biotechnology in Organ Repair (Ministry of Education), Shanghai University, Shanghai 200444, P. R. China

[#]These authors contributed equally.

Email: wangl@shu.edu.cn (L. Wang).

### Materials Characterization

Transmission electron microscopy (TEM, HT7700), high-resolution transmission electron microscope (HAADF-STEM, JEOL JEM-ARM200F), and atomic force microscope (AFM) from Bruker Dimension Icon AFM were employed in characterizing surface morphology. X-ray diffraction (XRD) patterns were marked by

Rigaku TTR-III using Cu K radiation. Raman spectra were operated on a Thermo Fisher Scientific DXRxi laser Raman spectrometer with excitation wavelength = 532 nm (0.1 mW). Fourier transform infrared (FT-IR) spectra were characterized on a Nicolet 5700 spectrophotometer over the range of 3500-500 $cm^{-1}$. X-ray photoelectron spectroscopy (XPS) was gathered using the Thermo Scientific K-Alpha x-ray photoelectron spectrometer. Electrochemical analyses were performed in the Autolab (1.0) electrochemical workstation.

**Contact angle measurement**

The contact Angle test results were used for characterizing the hydrophilicity of the material. The ground material was spread onto a slide and flatten. Subsequently, water droplets were deposited on the surface of the material. Once the water droplets stabilize on the material's surface, the sampling was stopped and the contact angle was calculated using software.

**Electrochemical measurements**

The 5 mg catalyst was dispersed in a mixed solution of 600 μL isopropanol, 400 μL water and 50 μL Nafion solution followed by ultrasonic treatment for 30 min. Then 10 μL solution was dropped onto the polished glassy carbon (GC) electrode (0.19625 $cm^2$) for testing. The electrochemical test was carried out in a three-electrode system with the prepared material as the working electrode, Ag/AgCl as the reference electrode and graphite rod as the counter electrode. The solution was keeping stirring (600 rpm) during the test. Linear sweep voltammetry (LSV) test was performed in an undivided cell. The LSV curves was collected after cycle voltammetry (CV) activation from 0.926 V to 1.826 V (vs. RHE) for 15 circles at 50 mV $s^{-1}$ in 1.0 M KOH and iR-compensation was applied in the measurement.

The formula used in the article is as follows:

$$E(RHE) = E(Ag/AgCl) + 0.0591\ pH + 0.1989\ V \quad (1)$$

The formula is used to convert reference electrode potential into reversible hydrogen

electrode potential in alkaline electrolyte with pH=14, E(Ag/AgCl) represents reference potential, and pH refers to the pH of the electrolyte.

**The measurement of electrochemical active surface area (ECSA)**

Electrochemical Active Surface Area (ECSA) refers to the portion of the electrode surface actively participate in electrochemical reactions, serving as a metric to evaluate Sthe true catalytic efficacy of the catalyst. The test voltage range was centered on the open circuit voltage and fluctuates up and down by 50 mV. The scanning rate of ECSA test was 20, 40, 60, 80, and 100 mV $s^{-1}$.

The ECSA was measured from the following equation

$$ECSA = \frac{C_{dl}}{C_s} \quad (2)$$

where the double-layer capacitance ($C_{dl}$) was determined from the cyclic voltammetry curve at different sweep speeds and slope was calculated by linear fitting. The value of the specific capacitance ($C_s$) was determined to be 0.04 mF $cm^{-2}$ (1.0 M KOH).

**The measurement of In-situ infrared spectroscopy**

*In-situ* infrared spectroscopy was performed under different potentials by an infrared spectrometer (Thermo Fisher, Nicolet iS50 FT-IR, USA) and CHI 760E electrochemical workstation. The electrolytic cell is an H-type divided cell separated by Nafion 117 membrane. The reference electrode is Ag/AgCl electrode; the counter electrode is the graphite rod electrode. The working electrode was prepared by dropping 1 mL solution (5 mg of catalyst, 500 μL of water, and 500 μL of isopropanol) onto a gas diffusion layer. After that, the carbon paper was cut into a circle with a diameter of 0.6 cm, and placed on the reflecting surface of the ATR silicon prism. The measurements were performed in 1.0 M KOH aqueous solution at 1.50 V vs. RHE. The signals were captured every 30 seconds throughout the entire process for 30 minutes, providing a comprehensive understanding of the samples' behavior.

**The measurement of In-situ Raman spectroscopy**

In-situ Raman spectroscopy was obtained by Raman microscope (HORIBA, XploRA PLUS, France) and CHI 660E electrochemical workstation in flow cell with 1.0 M KOH as the electrolyte, a 50× objective lens was used to focus the laser with 532 nm on the sample. The GDL electrode, Ag/AgCl electrode and Pt wire were used as the working electrode, the reference electrode, and the counter electrode, respectively. The measurement was performed under an exposure time of 4 s with an accumulation number of 20 times.

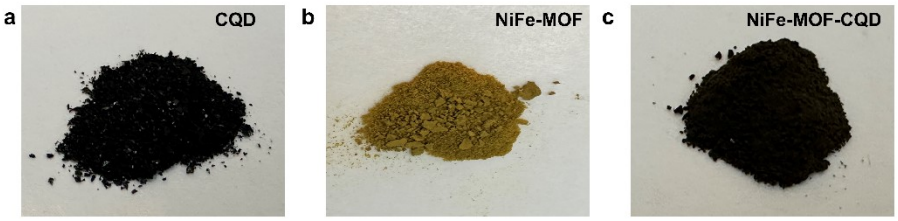


**Figure S1.** The photographs of (a) NiFe-MOF, (b) NiFe-MOF and (c) EW-CQD-MOF under daylight.

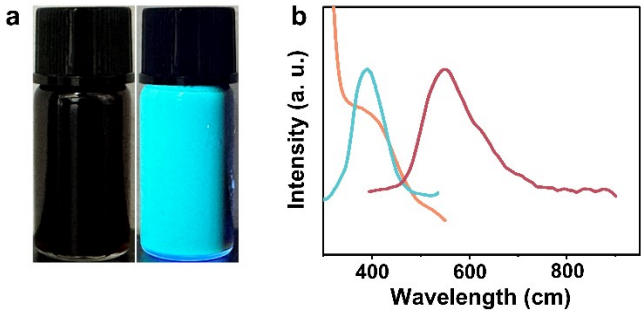


**Figure S2.** (a) The diagram and (b) ) the UV-vis, PL, and PLE spectra of CQD.

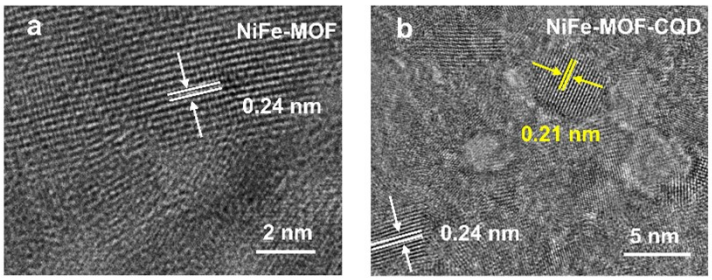

**Figure S3.** High-resolution TEM images of (a) NiFe-MOF and (b) NiFe-MOF-CQD.

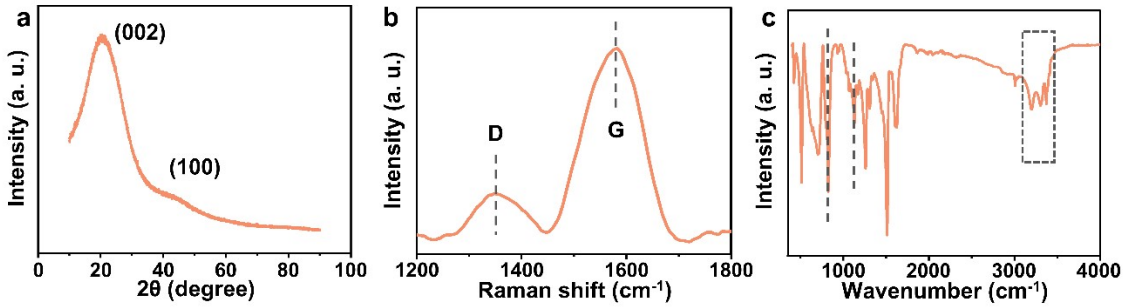


**Figure S4.** (a) XRD pattern, (b) Raman spectrum and (c) FT-IR spectrum of CQD.


**Figure S5.** Static contact angles of B-CQD-MOF and ED-CQD-MOF in the presence of $H_2O$

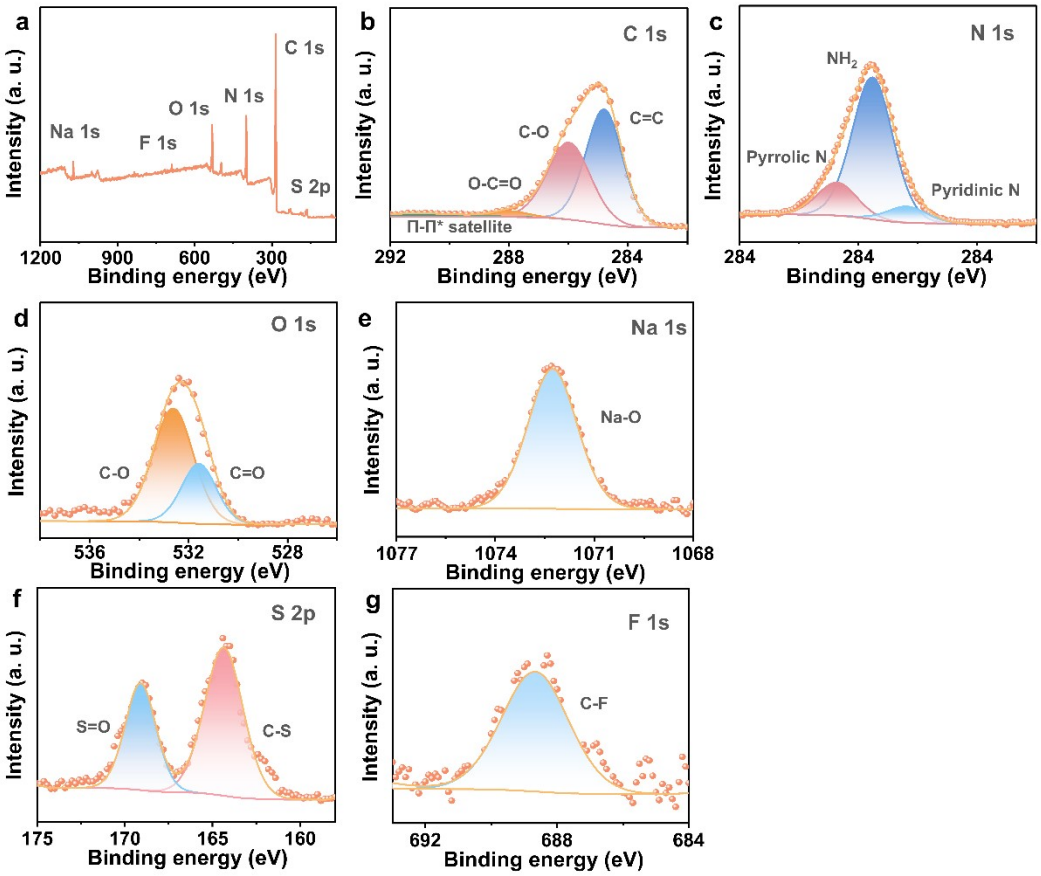


**Figure S6.** (a) XPS survey and high-resolution XPS (b) C 1s, (c) N 1s, (d) O 1s, (e) Na 1s, (f) S 2p and (g) F 1s of CQD.

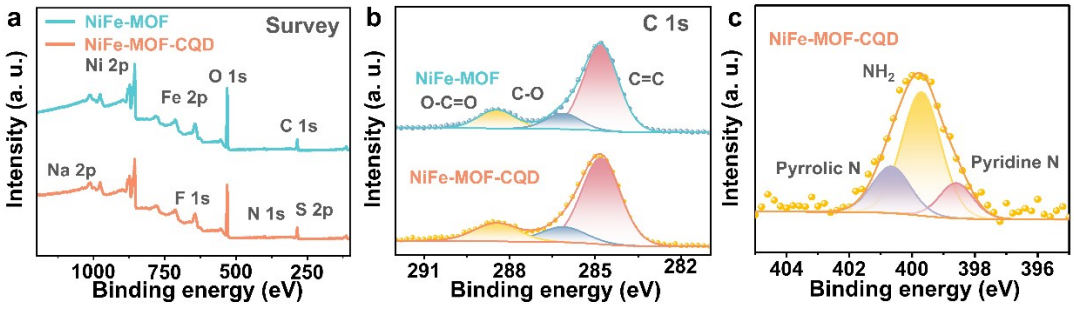


**Figure S7.** (a) XPS survey and high-resolution XPS (b) C 1s of NiFe-MOF and NiFe-MOF-CQD, (c) high-resolution XPS N 1s of NiFe-MOF-CQD.

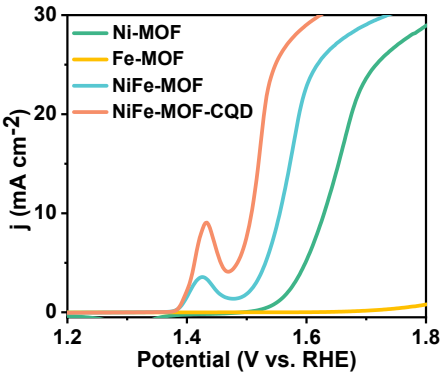


**Figure S8.** LSV curves of Ni-MOF, Fe-MOF, NiFe-MOF and NiFe-MOF-CQD in 1.0 M KOH.

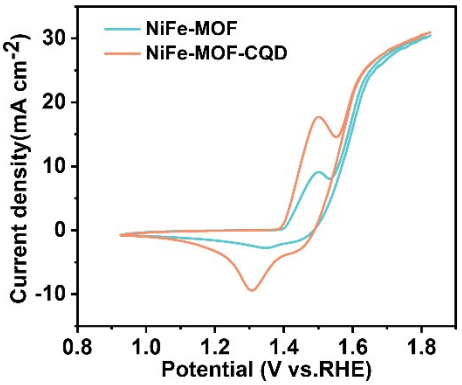


**Figure S9.** CV curves of NiFe-MOF and NiFe-MOF-CQD after 30 cycles from 0.9 to 1.8 V vs.RHE.

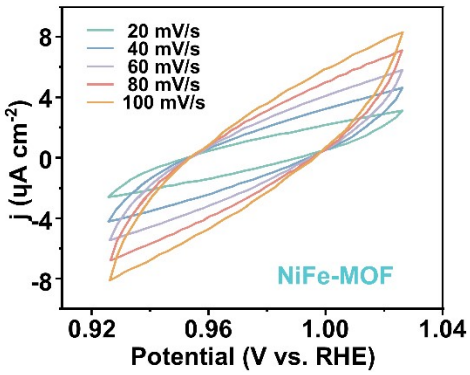


**Figure S10.** The CV curves for NiFe-MOF at different scan rates: 20, 40, 60, 80 and 100 mV/s from inside to outside.

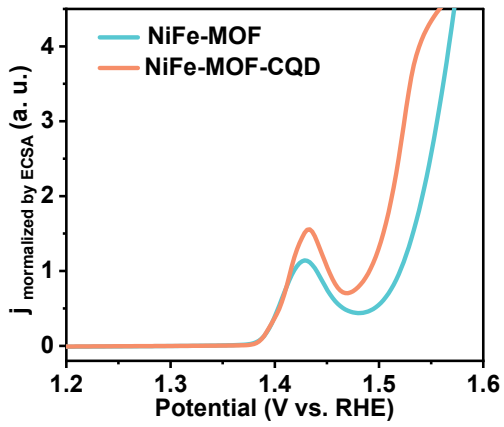


**Figure S11.** LSV curves normalized by ECSA of NiFe-MOF and NiFe-MOF-CQD.

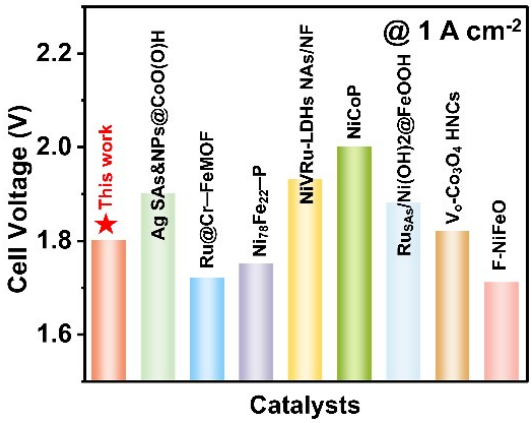


**Figure S12.** Comparison of cell voltage at 1 A $cm^{-2}$ at PEM electrolyzers using NiFe-MOF-CQD as anode with other reported catalysts.